PAPER

Removal of Pb-based compounds mediated by graphene oxide-like materials obtained from *Sargassum*: unravelling key features of their interaction using density functional theory and spectroscopic methods†

Sandra Julieta Gutierrez-Ojeda,[a] Rocío Martínez-Flores,*[b] Raúl Pareja-Rodríguez,[c]
Geonel Rodriguez-Gattorno,[c] Rodrigo Ponce-Pérez,*[d]
María G. Moreno-Armenta[d] and Jonathan Guerrero-Sánchez [ID][d]

Graphene oxide obtained from biomass possesses a rich variety of properties and applications. *Sargassum*, a macroalgae abundant in the Caribbean Sea, has been proposed as a viable and cost-effective biomass. Graphene oxide derived from *Sargassum* has an unprecedented selectivity for Pb capture in the hydrocerussite phase. This study presents exhaustive theoretical and experimental efforts to understand the interaction between Pb-based molecules (Pb, $Pb(CO_3)_3$, and $Pb(OH)_2$) with representative models of the functional groups present in graphene oxide (COOH, OOH, OH, and O). Our results demonstrate that CO_3 enhances the Pb adsorption on the graphene oxide surface. Hydrogen bonds and van der Waals interactions between CO_3 of the $Pb(CO_3)_3$ with the GO surface are the driving forces to improve the Pb capturing process and further hydrocerussite formation on GOs. Although Pb and $Pb(OH)_2$ can also be trapped by graphene oxide, it is less probable from an energetic point of view. Here, we demonstrate that low-cost graphene oxide obtained from *Sargassum* can be useful in environmental remediation.

Environmental significance

Graphene oxide (GO) obtained from *Sargassum* has demonstrated its viability in removing heavy metals such as Pb from water because of their intrinsic functional groups on their surface. Using *Sargassum* as a precursor of GOs, we can reduce their impact on Mexican coasts, and also, GOs help us to remove Pb^{2+} from water by the formation of hydrocerussite minerals.

Introduction

Water pollution is one of the most critical global challenges. Heavy metals are a major concern among water contaminants due to their toxicity and carcinogenic effects.[1] Also, they are not biodegradable and tend to bioaccumulate, increasing their concentration in living organisms. The most common water contaminants are those obtained from petroleum refineries and electronic waste: antimony (Sb), arsenic (As), cadmium (Cd), and chromium (Cr). Heavy metal contaminants such as mercury (Hg) and lead (Pb) mainly stem from pesticides, fertilizers, insecticides, and industrial waste.[2]

Lead ion (Pb^{2+}) is one of the most toxic ions since it can severely harm human bodies.[3,4] As a result, the efficient separation/removal of Pb^{2+} from aqueous solutions is critical and has attracted much attention.[5] Consequently, multiple approaches have been developed to remove Pb from water. For example, chemical precipitation,[6] ion exchange, and electrochemical removal.[7] However, the facilities, operation, and maintenance are significant disadvantages. Despite this, adsorption has been considered one of the most economical and standard methods in water purification. In this sense, oxygen-containing functional groups perform remarkably, such as carbon nanotubes, clay minerals, metal oxides, and bio-adsorbents.[8–13]

[a] *Instituto de Física, Universidad Nacional Autónoma de México, 04510 Ciudad de México, Mexico*

[b] *Tecnológico Nacional de México, TecNM, Instituto Tecnológico Superior de Monclova, Carretera 57 km. 4.5, 25733 Monclova, Coahuila, Mexico. E-mail: rocio.mf@monclova.tecnm.mx*

[c] *Departamento de Física Aplicada, CINVESTAV-IPN, Carr. Antigua a Progreso km. 6, CORDEMEX, 97310 Mérida, Yucatán, Mexico*

[d] *Centro de Nanociencias y Nanotecnología, Universidad Nacional Autónoma de México, Km. 107, Apdo. 14 Carretera Tijuana, Ensenada, Baja California, Mexico. E-mail: rponce@ens.cnyn.unam.mx*

† Electronic supplementary information (ESI) available: Less stable DFT models, O 1s XPS, GO-Pb EDS, and XRD. See DOI: https://doi.org/10.1039/d4en00301b

4372 | *Environ. Sci.: Nano*, 2024, **11**, 4372–4380

This journal is © The Royal Society of Chemistry 2024

Graphene oxide (GO), consisting of a hexagonal network of covalently bonded carbon (C) atoms, has attracted multidisciplinary research due to its two-dimensional structure and unique physicochemical properties.[14] GOs with oxygen-containing functional groups are very suitable for pollutant trapping due to their excellent remotion ability.[15,16] GOs can be obtained by conventional thermal decomposition of biomass.[17,18] Surprisingly, GOs from *Sargassum* sp. have shown impressive Pb^{2+} absorption capacities by forming a very stable mineral phase known as hydrocerussite.[19] This is unexpected since GOs from *Sargassum* tend to have a high calcium concentration, which supposedly interferes with lead absorption.[20] Understanding the carbonaceous residue interaction with Pb^{2+} is important because they are the primary materials for removing this toxic metal. In this way, Pareja-Rodríguez *et al.*[19] suggest that the interface displays high interaction with Pb^{2+} in aqueous solutions due to functional groups (OH, C–O, CO_3). They suggested that the functional groups in GOs obtained from *Sargassum* play an important role in Pb^{2+} removal because of their interaction with CO_3 groups, inducing a hydrophilic character and chemical reactivity superior to graphene. However, an atomic scale analysis to understand how Pb-based compounds from hydrocerussite minerals are removed has yet to be reported.

With this precedent, we investigate the Pb-based compounds' remotion mechanisms by GOs using quantum mechanics calculations in combination with experimental characterization techniques: Raman, infrared (FTIR), and X-ray photoelectron spectroscopy (XPS). We account for Pb^0, $Pb(CO_3)_3$, and $Pb(OH)_2$ molecules (in which Pb is a cation Pb^{2+}) adsorbed on the GO functionalized surface. The results denote that the unique features of some functional groups in GOs obtained from *Sargassum* allow Pb^{2+} capture, generating H bonds and weak van der Waals interactions that enhance the surface interaction and hydrocerussite growth on the functionalized monolayer.

Methods

Computational methods

The adsorption of Pb^0, $Pb(CO_3)_3$, and $Pb(OH)_2$ onto GOs was studied by DFT calculations in the absence of temperature. The calculations were done using the Vienna *Ab initio* Simulation Package (VASP)[21–23] code. The electronic states were expanded using the projector-augmented wave (PAW) basis[24,25] with a cutoff energy of 480 eV. The exchange–correlation energies were treated using the generalized gradient approximation (GGA) with the Perdew–Burke–Ernzerhof (PBE) parametrization.[26] The DFT-D3 correction of Grimme is adopted to describe the van der Waals (vdW) interaction.[27] The GOs were simulated using the supercell method. Since our calculations are periodic, the supercell includes a vacuum space perpendicular to graphene larger than 15 Å to avoid interaction between periodic slabs. Also, the supercell is formed by 5 graphene

unit cells of length along the x and y axis to form a $5 \times 5 \times 1$ periodicity. In the geometry optimization, the convergence criterion for all force components must be less than 0.026 eV Å^{-1} and total energy differences are less than 1×10^{-4} eV. The Brillouin zone is sampled with a gamma-centered k-points grid of $7 \times 7 \times 1$, employing the Monkhorst–Pack scheme.[28] Non-covalent interactions were calculated using the CRITIC2 software.[29] For more details about parameter optimization, see the ESI.†

Experimental characterization techniques

The Raman spectra were obtained using an Alpha 300 WITEC equipment (ALPHA 300RA, Lise-Meitner, Germany), utilizing a Ne (blue) laser with a λ = 488 nm. To ensure the safety of the samples, the laser power was maintained below 10 mW throughout the measurements to prevent potential sample damage caused by laser irradiation. X-ray photoelectron spectroscopy analysis was conducted using a K-Alpha Thermo Scientific (XPS, Waltham, USA) spectrometer with an Al Kα X-ray monochromatic source (1486.6 eV) at 12 kV and 40 W. The analyzed area was 400 μm^2, using an incident relative angle of 30°. Before analysis, the surface of the samples was treated by argon (Ar) erosion for 30 s (3 kV and 30 W). The deconvolution of the XPS spectra was performed with different mathematical functions (Lorentzian, Gaussian, and their combinations). X-ray diffraction patterns were collected using a Bruker D-8 Advance diffractometer (Bruker, Billerica, USA) operating at 40 kV and 30 mA in the angular range 5–60° at a step interval of 0.02° and a counting time of 0.5 s with Cu-Kα$_1$ radiation.

Results and discussion

First, the graphene monolayer was optimized from scratch. Our calculated cell parameter is a = 2.47 Å, which agrees with previous reports.[30] Since pristine graphene is not reactive, H, O, or OH functionalized graphene promotes active sites, conferring physicochemical properties suitable for Pb-based compound removal. Characterization techniques allowed us to differentiate the geometries of carbon atoms and detect the presence of functional groups (OH, C–O, C=O, COOH, and CO_3^{2-}). All these functional groups may provide the chemical characteristics to GOs for acting as a very efficient adsorbent material.

Previously, Paez-Ornelas *et al.*[31] reported four stable GO configurations containing COOH, OH, and O functional groups. We reproduce their models from scratch using a graphene layer. The atomic representation of the structures can be seen in Fig. 1, where the models are labeled as C1, C2, C3, and C4. These models align with the experimentally observed functional groups, so we use them to study the Pb-based compound capture.

The adsorption energy (E_{ads}) of the functional groups or Pb-based molecules follows the equation:

$$E_{ads} = E_{slab} - E_{ref} - E_{funct\ group/molecule} \qquad (1)$$

This journal is © The Royal Society of Chemistry 2024

Environ. Sci.: Nano, 2024, **11**, 4372–4380 | **4373**

Fig. 1 Top and side views of the four GO atomic models. a) C1, b) C2, c) C3, and d) C4. Brown, red, and white spheres represent C, O, and H atoms.

where E_{slab} is the energy of the system under study, E_{ref} is related to the defected or functionalized (O, H, and OH) graphene monolayer, and $E_{funct\ group/molecule}$ corresponds to the energy of the isolated functional group or molecule. Negative values suggest favorable adsorption, while positive values evidence non-favorable adsorption. The E_{ads} for the different functional groups onto GOs are −9.12 eV, −3.71 eV, −4.58 eV, and −8.08 eV for C1, C2, C3, and C4 configurations.

Although E_{ads} allows us to see that all functional groups favorably adsorb on the graphene sheet, and we cannot compare the stability of these models since they have a different number of atoms. In this way, the defect formation energy (DFE) formalism – that does not depend on the number of atoms but on the chemical potentials – is appropriate to describe our system's stability.[32–34] The DFE is defined as

$$DFE = \frac{E_{slab} - E_{clean\_GO} - \sum n_x \mu_x}{A} \quad (2)$$

where A is the area of the system under study, E_{slab} is the total energy of the system under study, E_{clean_GO} is the energy of the partially passivated GOs, n_x accounts for the number of x adsorbed atoms, and μ_x is the chemical potential of the x atom-defined as $\mu_x = E^x/n$, where E^x is the total energy of the x element in their most stable bulk/molecular configuration and n is the number of atoms present in the unit cell. The lowest DFE values indicate the most stable model. The DFEs for each functional group C1, C2, C3, and C4 are −0.09 eV Å^{-2}, −0.17 eV Å^{-2}, −0.09 eV Å^{-2}, and −0.08 eV Å^{-2}, respectively. Notice that C2 is the most stable configuration, in agreement with Paez-Ornelas et al.[31]

Experimentally, a flake shape is observed when the Pb^{2+}-containing moieties are adsorbed on GOs.[19] The flake shape on the surface is similar in morphology to hydrocerussite ([Pb$_3$(CO$_3$)$_2$(OH)$_2$]), as reported by Siidra et al.[35] This mineral has unit cell parameters of $a = 5.248(3)$ and $c = 23.66(1)$ Å. Additionally, it has the space group $R\bar{3}m$ with Wyckoff positions 6c and 18h for Pb1 and Pb2, respectively.

To understand the Pb-based compound adsorption process on the GOs, we accounted for the hydrocerussite constituents: the mineral cerussite, Pb(CO$_3$), and Pb(OH)$_2$ sheets, which contain OH groups and Pb^{2+}. So, the isolated Pb^0 and the molecules Pb(CO$_3$)$_3$ (see the ESI† for more

details) and Pb(OH)$_2$ are adsorbed on the four possible functional groups in the GOs. Fig. 2 shows the atomic configurations of the molecules considered in this work. The treated constituents from the hydrocerussite cif file were simulated in a cubic box of 20 Å.

Table 1 summarizes the DFE values for the Pb^0, Pb(CO$_3$)$_3$, and Pb(OH)$_2$ molecules adsorbed on the four GO models. For each molecule adsorbed in a different functional group, we consider different orientations for the interaction to find the most stable configuration; in the manuscript, we focus on the most stable model for each case.

First, we focus on the isolated Pb^0. Regarding the COOH functionalized GOs (C2 model), Pb^0 can interact with the O from the CO or the OH group. The interaction with the CO group is the most favorable configuration with a DFE value of −0.16 eV A^{-2}. The atomistic representation of this configuration is depicted in Fig. 3a. Here, Pb^0 bonds to O from the carbonyl group with a bond distance of 2.25 Å. Also, the surface–Pb separation distance is 2.82 Å. These results show that Pb–O bonds are stable on GOs. The C1, C3, and C4 configurations display higher defective formation energies (−0.10 eV Å^{-2}, −0.06 eV Å^{-2}, −0.07 eV Å^{-2}, respectively), and are schematized in Fig. S3 of the ESI.†

In the case of the Pb(CO$_3$)$_3$ molecule (Pb^{2+}), the most stable interaction is with the C2 GO configuration with a DFE of −0.66 eV Å^{-2}. Here, the adsorption takes place in the carbonyl group. Also, we notice a ligand exchange between the OH group from GOs and one of the carbonate groups of the Pb(CO$_3$)$_3$ molecule. After the interaction, Pb is still sixfold coordinated, retaining the stability of the Pb^{2+} moiety, as shown in Fig. 3b. The Pb1–O bond distance is 2.25 Å, while the distance between the surface and the Pb1 atom is 4.57 Å. Although the C1 functional group is similar to C2, the Pb(CO$_3$)$_3$ adsorption on the C1 site is less stable by 0.08 eV Å^{-2}, probably because ligand exchange does not happen spontaneously compared to the C1 site. Also, as the COOH functional group in C1 is formed in C of the graphene structure, steric effects may induce the large formation energy.

On the other hand, C3 and C4 sites are less stable by 0.07 eV Å^{-2} and 0.11 eV Å^{-2}, respectively. In C3, ligand exchange
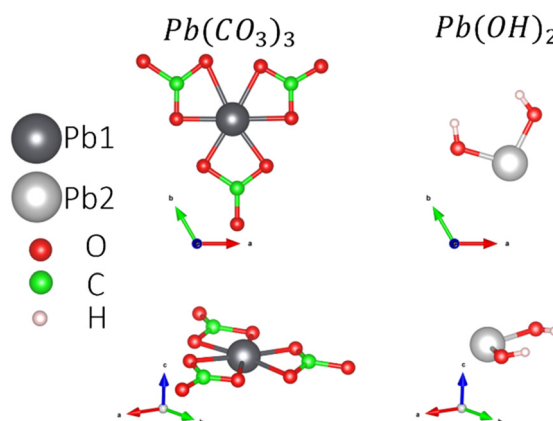

Fig. 2 Atomistic models of the hydrocerussite constituents.

Table 1 DFE values for the adsorption of Pb^0, $Pb(CO_3)_3$, and $Pb(OH)_2$ molecules onto C1, C2, C3, and C4 GO configurations

GO configuration	DFE (eV Å^{-2})		
	Pb^0	$Pb(CO_3)_3$	$Pb(OH)_2$
C1	−0.10	−0.58	−0.25
C2	−0.16	−0.66	−0.30
C3	−0.06	−0.59	−0.22
C4	−0.07	−0.55	−0.20

appears; however, there is no evident chemical interaction between Pb and O, which is the main reason behind the lower DFE. Finally, C4 is the site with the larger DFE because weak vdW interactions hold the O–$Pb(CO_3)_3$ interaction. Although the C1, C3, and C4 functional groups are less stable, experimentally, it has been shown that they may participate under N and air atmospheres.[19] Considering the previous results, COOH groups are the most prominent for Pb^{2+} adsorption on GOs.[5] Fig. S4† shows the less stable models for $Pb(CO_3)_3$ adsorption.

Finally, we analyze the adsorption of the $Pb(OH)_2$ molecule (Pb^{2+}) on the different GO models. The DFE displays that the C2 configuration, again, is the most stable due to the interaction between an H atom from the COOH group and the OH group from the $Pb(OH)_2$ molecule, generating a physisorbed H_2O molecule and chemical O–Pb–O bonds with distances of 2.43 Å and 2.38 Å with the COO functional group (see Fig. 3c). Also, the Pb2–surface distance is 5.03 Å. When the molecule is adsorbed on C1, the DFE is higher. In this case, an H_2O molecule is generated due to the ligand exchange between the OH group of the C1 functional group and one OH of the $Pb(OH)_2$ molecule. The H_2O molecule interacts through weak vdW interactions with one O atom of the COO group, and the Pb attaches to the

remaining O atom. The main difference between C1 and C2 is the Pb bonding; in C1, it forms one bond, while in C2, it is two-fold coordinated. $Pb(OH)_2$ adsorption on C3 and C4 sites shows less stable DFEs by 0.08 eV Å^{-2} and 0.10 eV Å^{-2}, respectively. See Fig. S5† for structural details of the unstable adsorption sites. Table 2 summarizes the bond distances obtained in the most stable cases for each molecule.

Upon analyzing all the possible adsorption sites for the Pb-based molecules on the different functional groups, we noticed that the C2 configuration is the most viable configuration to trap Pb through oxygen interaction and ligand exchange. As evidenced in the experiment, all the functional groups trap Pb, however, COOH is the most efficient and desirable for its removal.

To identify the different kinds of interactions present in the adsorption of Pb^0, $Pb(CO_3)_3$, and $Pb(OH)_2$ on COOH functionalized GO surface, we investigate the non-covalent interactions (NCIs).[36,37] The NCI is a useful tool that helps us distinguish between the different interactions in our systems. We investigated the NCIs by calculating the reduced density gradient, $s[\rho(r)]$:

$$s[\rho(r)] = \frac{1}{2(3\pi^2)^{\frac{1}{3}}} \frac{|\nabla\rho(r)|}{\rho(r)^{\frac{4}{3}}} \tag{3}$$

also, the sign of the Laplacian of the density ($\nabla^2\rho(r)$) is useful to distinguish between different types of interactions. To better understand the interactions in the system, the Laplacian is decomposed into a sum of contributions. These components are the three eigenvalues (λ_i) of the electron density Hessian. The sign of the second eigenvalue (λ_2) is useful to differentiate the different interactions present. Negative values ($\lambda_2 < 0$) denote bonding interactions, while positive values ($\lambda_2 > 0$) are for nonbonded interactions; also,
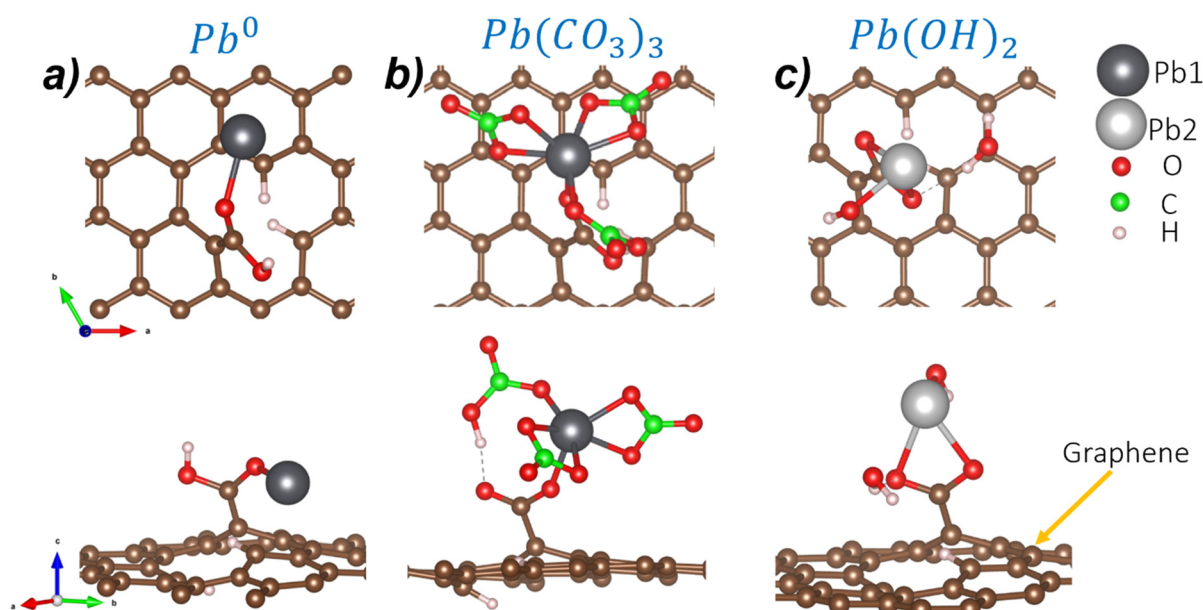

Fig. 3 The most stable adsorption configurations for a) Pb^0, b) $Pb(CO_3)_3$, and c) $Pb(OH)_2$ molecules.

This journal is © The Royal Society of Chemistry 2024

Environ. Sci.: Nano, 2024, **11**, 4372–4380 | **4375**

Table 2 Structural details for the Pb^0, Pb(CO$_3$)$_3$, and Pb(OH)$_2$ adsorption on the most stable configuration

System	Bond length (Å)				
	Pb1–O	Pb2–O	Pb2–OH	Pb1–surface	Pb2–surface
C2–Pb^0	2.25	—	—	2.82	—
C2–Pb(CO$_3$)$_3$	2.23	—	—	4.57	—
C2–Pb(OH)$_2$	—	2.43	2.13	—	5.03

values close to zero ($\lambda_2 \approx 0$) evidence weak interactions (van der Waals).

Fig. 4 exhibits the NCI index for the adsorption of Pb and Pb compounds on the GOs. Fig. 4a displays their corresponding isosurface (s = 0.5 a.u), where blue isosurfaces show attractive interactions, red color indicates repulsive interactions, and green isosurfaces are vdW interactions. The results show attractive interaction between Pb and O from COOH; similar behavior is noticed between Pb and the GO surface, and vdW forces are noticed around the attractive interaction. Fig. 4b shows the $s[\rho(r)]$ *vs.* sign(λ_2)$\rho(r)$ plot, where the purple surface denotes all the interactions in the system and the green surface represents the Pb–surface interaction. We focus on the low s and low ρ regions to distinguish the non-covalent interactions. The sharp peak observed at −0.07 corresponds with the bond Pb–O formed after the interaction, while the peak at −0.05 is attributed to the interaction that ocuurs between Pb and graphene. Also, the green surface at low s and close to zero ρ indicates vdW interactions between Pb and the surface.

Their corresponding isosurfaces (s = 0.5 a.u.) and $s[\rho(r)]$ *vs.* sign(λ_2)$\rho(r)$ graph for the adsorption of Pb(CO$_3$)$_3$ molecule on the COOH functionalized GOs are displayed in Fig. 5a and b respectively. In the graph, the purple color surface denotes all the interactions in the system. After the ligand exchange reaction, the blue sharp peak at −0.05 is for the H bond formed between a CO$_3$ and the COOH functional group. Fig. 5a shows that the H bond has an attractive character. The sharp orange peak at 0.075 corresponds to the Pb–O interaction, and the result suggests that the bond formed is ionic. The vdW interactions between the CO$_3$ groups and the surface are seen in Fig. 5a, denoted by the

green isosurface. This is corroborated in Fig. 5b, where the green surface is observed at low s and low ρ.

Regarding the Pb(OH)$_2$ adsorption, their corresponding isosurface (s = 0.5 a.u.) and $s[\rho(r)]$ *vs.* sign(λ_2)$\rho(r)$ plot are depicted in Fig. 6a and b, respectively. Pb interacts with the COOH functional group by forming two Pb–O bonds, corresponding with the sharp peaks at −0.05 and 0.06, after a ligand exchange reaction producing a water molecule. The water molecule still interacts with the Pb molecule and the GO surface by weak interactions. Also, according to Fig. 6a, a kind of H bond interaction between the O from COO and the H from H$_2$O has a repulsive character. Such interaction corresponds to the sharp peak at 0.03 in Fig. 6b.

Experimental characterization

The graphene oxide derived from *Sargassum* sp. was obtained by thermal decomposition at 420 °C without atmosphere control, as previously reported by Pareja-Rodríguez *et al.*[19] As a result, they observed the presence of OH, C–O, C═O, C–OH and CO$_3^{2-}$ functional groups onto GOs. As proof of concept, we study the GOs after the interaction with the Pb-based compounds using spectroscopic techniques such as Raman and XPS. The results are shown in Fig. 7. The Raman spectra (see Fig. 7a) show the typical pattern of the graphene oxide-like materials.[38] However, compared with the GOs without interaction with Pb^{2+} reported by Pareja-Rodríguez *et al.*,[19] we notice the new bands at 562 and 1088 cm^{-1}, indicating the presence of vibrational modes associated with –(COO)Pb bonds.[5,39] These vibrations suggest the formation of bonds between the GOs functional groups and Pb^{2+} ions *via* the coordination or complexation with the carboxylate (COO$^-$) groups.
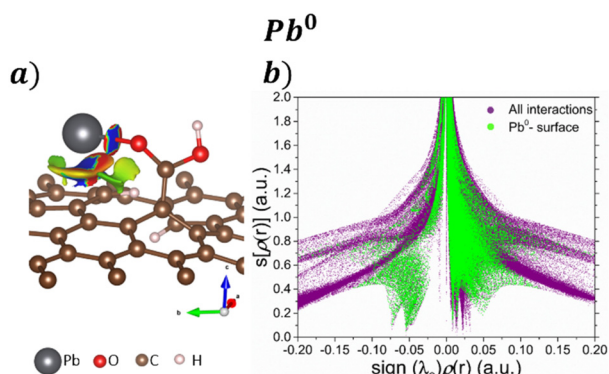

Fig. 4 a) NCI isosurfaces with s = 0.05 a.u. and their corresponding b) $s[\rho(r)]$ *vs.* sign(λ_2)$\rho(r)$ graph for the adsorption Pb^0 on the GO surface.

Fig. 5 a) NCI isosurfaces with s = 0.05 a.u. and b) $s[\rho(r)]$ *vs.* sign(λ_2)$\rho(r)$ graph for the adsorption Pb(CO$_3$)$_3$ on the GO surface.

4376 | *Environ. Sci.: Nano*, 2024, **11**, 4372–4380
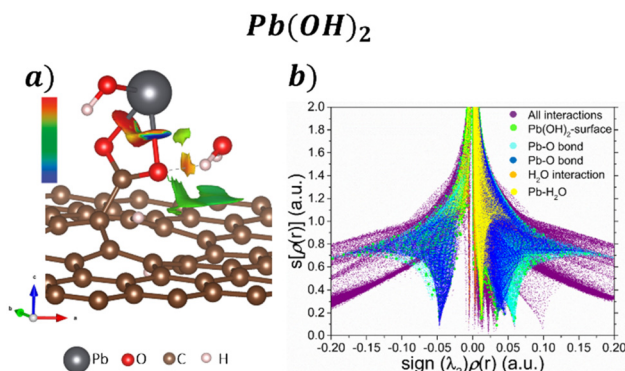
This journal is © The Royal Society of Chemistry 2024

Fig. 6 a) NCI isosurface with $s = 0.05$ a.u. and b) $s[\rho(r)]$ $vs.$ sign$(\lambda_2)\rho(r)$ graph for the adsorption Pb(OH)$_2$ on the GO surface.

Fig. 7 Experimental characterization of GO–Pb^{2+}: a) Raman, b) O 1s, and c) Pb 4f high-resolution XPS spectra.

Additionally, the G peak position shift from 1538 to 1585 cm^{-1} can be attributed to physical stress and electron transfers between functional groups of the GOs (mainly COOH) and Pb^{2+} ions.[5] The G peak shift towards higher values indicates that GOs experience an increase in electron density. This shift suggests that the interaction with Pb^{2+} leads to an alteration in the electronic environment of the GOs, potentially due to electron transfer from the functional groups to the GO structure.[5,40] The observed changes in the Raman spectrum of GOs provide clear evidence of chemical modifications occurring on their surface; these changes highlight the surface reactivity of GOs and the formation of new chemical species due to interaction with Pb^{2+} ions.

Pareja-Rodríguez et al.[19] provided the FTIR spectra of GOs before and after interacting with Pb^{2+} ions. The bands in 1421, 874, and 711 cm^{-1} are mainly associated with carbonates (CaCO$_3$).[19,41] The slight change in the position and intensity of the carbonate-related bands after the interaction with Pb^{2+} justifies the theoretical calculations since weak interactions dominate. The carbonates are not the main active sites on the GO surface for interacting with Pb^{2+} ions. The band at 1105

cm^{-1}, associated with C–O stretching vibrations of COOH groups,[5,19] decreases appreciably in intensity and shifts to lower wavenumber values, indicating the formation of chemical bonds with an element of highly reduced molecular mass such as Pb. Such a shift towards lower wavenumbers may indicate a change in the chemical environment, suggesting the involvement of the COOH groups in the interaction with Pb^{2+} ions. According to Raman spectroscopy, the interaction between the COOH groups and Pb^{2+} ions can form –(COO)Pb bonds. These results support the theoretical calculations demonstrating that COOH groups are active sites where the Pb^{2+} ions adsorb on the GO surface.

To evaluate the chemical bonding state of the GO surface after Pb interaction, XPS analysis was performed. The high-resolution O 1s spectra (Fig. 7b) show three individual components located at 533.3, 531.3, and 529.7 eV that corresponds with the signal of carboxylic groups (COOH),[5,42] the presence of O bonded to tetrahedral carbon (O–Csp^3),[5,42] associated with ethers and alcohols (C–O–C and C–OH), and the O bonded to Pb (O–Pb),[43] respectively. Besides, Fig. S6† displays the high-resolution O 1s spectra before the adsorption of Pb-based molecules. Notice a shift to higher bond energies – after the adsorption of Pb – of the peaks associated with the COOH groups and the C–O–C and C–OH groups, which supposes a change in the electron population in the GOs because of the presence of a massive atom such as Pb.

Table 3 presents the main functional groups' relative proportions. In GOs, the main oxygenated groups (in order of their relative proportion, calculated by the area under the curve of each component in the O 1s spectrum) promote multifunctional character and defects in their structure. The surface oxygen content (sOc) is related to the rigidity of graphene materials. Graphene oxide with a high sOc is very flexible, whereas reduced graphene oxide with a lower sOc has higher rigidity.[44] After interaction with lead, the formation of O–Pb bonds is observed,[5] and an important decrease (from 9.35 to 5.14%) in the relative proportion of COOH groups coincides with the theoretical prediction that these are the groups where the interaction with Pb-based compounds is more favored. This interaction between Pb-based compounds and the COOH groups could lead to a redistribution of electron density within the functional groups, decreasing electron density on the oxygen atoms forming the COOH groups. The presence of Pb^{2+} cations can induce polarization of electron density due to their positive charge. This electronic interaction can cause a redistribution

Table 3 Relative proportion of functional groups before and after GO and Pb^{2+} ions interaction

Before			After		
GOs	A (u^2)	RP (%)	GO–Pb	A (u^2)	RP (%)
C=O	10 121.88	2.35	O–Pb	15 946.60	3.64
C–O	92 606.80	21.53	C–O	93 541.00	21.32
COOH	40 218.65	9.35	COOH	22 526.16	5.14
O1s (total)	430 057.64			438 645.93	

This journal is © The Royal Society of Chemistry 2024

Environ. Sci.: Nano, 2024, 11, 4372–4380 | 4377

of electron density within the COOH group, leading to a decrease in electron density at the oxygen atoms and an increase in the binding energy.[5,42]

The high-resolution Pb 4f spectrum (Fig. 7c) displays two peaks, Pb $4f_{7/2}$ and Pb $4f_{5/2}$ at 138.4 and 143.2 eV, respectively. The Pb $4f_{5/2}$ signal is decomposed in two peaks at 143.2 eV, attributed to the COO^--Pb^+ species, indicating the presence of Pb^{2+} coordinated with carboxylate groups (COO^-).[5,42] The small peaks at 141.4 and 136.6 eV are associated with Pb^0 species due to photon-induced surface damage.[43] The peak at this binding energy suggests that a minor amount of metallic lead is present (as observed in the EDS mapping in Fig. S7†) on the surface of the GO–Pb. The Pb $4f_{7/2}$ peak at 138.4 eV, corresponds to COO^--Pb^+ species,[5,42] and another peak with a minor relative proportion at 137.5 eV corresponds to $Pb-CO_3$ bonds,[43] and this is consistent with the deconvolution of the O 1s peak. The higher relative proportion of the species (COO^--Pb^+) explains why most Pb^{2+} ions and the GO surface interactions are *via* carboxylic (COOH) groups.

Proposed mechanisms of Pb^{2+} adsorption

Once we have enough experimental and theoretical information about the adsorption of Pb^{2+} onto GOs, we propose the next adsorption mechanism.

Carboxylic groups ($-COOH^-$) and carbonate (CO_3^{2-}) on the surface of GOs contain oxygen atoms that can form chemical bonds with Pb^{2+}. These active sites facilitate the chemisorption of Pb^{2+} onto the GO surface through attractive forces and the formation of coordination bonds (COO^--Pb^+):

$$-COOH^- + Pb^{2+} \rightarrow -COOPb^+ + H^+ \quad (4)$$

The oxygen atoms in carboxylic groups can mainly act as intermediates, providing lone electron pairs to form coordination complexes with Pb^{2+} ions, reported as intermediate acids.[45] This classification is due to the conjugation of COOH groups with aromatic structures typical of graphene-like materials. In graphene-like materials, the carboxylate ions are conjugated with the aromatic structure. This conjugation stabilizes the negative charge on the carboxylate ion, making it less likely to accept protons (H^+) and behave as a base. Conjugation in the aromatic system influences the electron density distribution and the COO^- group reactivity, leading to its classification as an intermediate base.[45] There is an affinity between intermediate acids and hard bases, justifying the attractive interaction.

A chemisorption mechanism carries out the removal process of the Pb^{2+} ions due to electrostatic attractions between the Pb^{2+} ions and the GO surface functional groups in a basic medium (pH = 8.7, determined using a pH meter); this promotes the precipitation of $Pb(OH)_2$, as can be seen in the logarithmic distribution diagram presented in Fig. S8† generated according to the experimental conditions reported by Pareja-Rodríguez *et al.*[19] The effect of the increase of the

ionic strength, the product of the solubility of the salts contained in the GOs, and the presence of Cl^- ions increases the dissociation of this precipitate because of the functional groups on the surface; then hydrocerussite is formed. The solubility of this type of lead hydroxo-carbonate has been reported by Fiorito *et al.*;[41] its formation presupposes a considerable free energy change in the system, justifying the spontaneous transition of hydroxide to hydroxo-carbonate. The formation of this compound can be described as:

$$3PbOH^+ + 2CaCO_3 \rightarrow Pb_3(CO_3)_2(OH)_2 + 2Ca^{2+} + OH^- \quad (5)$$

After GOs interact with Pb^{2+} ions, the GO–Pb^{2+} system was analyzed by XRD (Fig. S9†). Our results reveal the presence of multiple crystallographic planes, in agreement with the PDF (Powder Diffraction File) entry 00-013-0131, which corresponds to the presence of hydrocerussite $[Pb_3(CO_3)_2(OH)_2]$.

Conclusions

To investigate the Pb^{2+} remotion and hydrocerussite formation using graphene oxide obtained from *Sargassum* sp. we focused on understanding the experimentally identified hydrocerussite mineral component (Pb^0, $Pb(CO_3)_3$, $Pb(OH)_2$) interaction with graphene oxide models (functionalized with COOH, OH, and O). The formation energy indicates that the COOH functional group is the most stable. Pb adsorption is through the oxygen atom in the COOH group. To understand the chemical interaction between the adsorbed molecules and the GO surface, non-covalent interactions (NCIs) were calculated. The NCI depicts that the CO_3 has van der Waals-like weak attractive interactions that enhance the Pb adsorption on the GO surface. However, repulsive and attractive interactions are present in $Pb(OH)_2$; this consolidates the idea that the presence of CO_3 enhances the Pb^{2+} removal process. Therefore, using *Sargassum*-based GOs is efficient for Pb^{2+} removal through hydrocerussite formation.

Author contributions

The manuscript was written through the contributions of all the authors. All the authors have approved the final version of the manuscript.

Conflicts of interest

There are no conflicts to declare.

Acknowledgements

4378 | *Environ. Sci.: Nano*, 2024, **11**, 4372–4380

This journal is © The Royal Society of Chemistry 2024

their technical support and useful discussions. All authors thank J. I. Paez-Ornelas for the table of contents image and useful comments and discussions.

Notes and references

1 C. Zamora-Ledezma, D. Negrete-Bolagay, F. Figueroa, E. Zamora-Ledezma, M. Ni, F. Alexis and V. H. Guerrero, Heavy metal water pollution: A fresh look about hazards, novel and conventional remediation methods, *Environ. Technol. Innovation*, 2021, **22**, 101504.

2 S. T. Song, N. Saman, K. Johari and H. Mat, Removal of Hg(II) from Aqueous Solution by Adsorption Using Raw and Chemically Modified Rice Straw As Novel Adsorbents, *Ind. Eng. Chem. Res.*, 2013, **52**, 13092.

3 M. L. Sall, A. Karim, D. Diaw, D. Gningue-Sall, S. E. Aaron and J. J. Aaron, Toxic heavy metals: impact on the environment and human health, and treatment with conducting organic polymers, a review, *Environ. Sci. Pollut. Res.*, 2020, **27**, 29927.

4 R. A. Goyer, Toxic and essential metal interactions, *Annu. Rev. Nutr.*, 1997, **17**, 37.

5 M. T. Nguyen, J. Zhang, V. Prabhakaran, S. Tan, E. T. Baxter, V. Shutthanandan, G. E. Johnson, R. Rousseau and V. A. Glezakou, Graphene Oxide as a Pb(II) Separation Medium: Has Part of the Story Been Overlooked?, *JACS Au*, 2021, **1**, 766.

6 O. Surucu, Trace determination of heavy metals and electrochemical removal of lead from drinking water, *Chem. Pap.*, 2021, **75**, 4227.

7 Q. Chen, Y. Yao, X. Li, J. Lu, J. Zhou and Z. Huang, Comparison of heavy metal removals from aqueous solutions by chemical precipitation and characteristics of precipitates, *Journal of Water Process Engineering*, 2018, **26**, 289.

8 C. L. Chen, X. K. Wang and M. Nagatsu, Europium Adsorption on Multiwall Carbon Nanotube/Iron Oxide Magnetic Composite in the Presence of Polyacrylic Acid, *Environ. Sci. Technol.*, 2009, **43**, 2362.

9 X. Ren, C. Chen, M. Nagatsu and X. Wang, Carbon nanotubes as adsorbents in environmental pollution management: A review, *Chem. Eng. J.*, 2011, **170**, 395.

10 A. Sarı, M. Tuzen and M. Soylak, Adsorption of Pb(II) and Cr(III) from aqueous solution on Celtek clay, *J. Hazard. Mater.*, 2017, **144**, 41.

11 C. Chen, X. Yang, J. Wei, X. Tan and X. Wang, Eu(III) uptake on rectorite in the presence of humic acid: A macroscopic and spectroscopic study, *J. Colloid Interface Sci.*, 2013, **393**, 249.

12 R. Zhang, C. Chen, J. Li and X. Wang, Investigation of interaction between U(VI) and carbonaceous nanofibers by batch experiments and modeling study, *J. Colloid Interface Sci.*, 2015, **460**, 237.

13 J. Li, X. Wang, G. Zhao, C. Chen, Z. Chai, A. Alsaedi, T. Hayat and X. Wang, Metal–organic framework-based materials: superior adsorbents for the capture of toxic and radioactive metal ions, *Chem. Soc. Rev.*, 2018, **48**, 2322.

14 X. M. Huang, L. Z. Liu, S. Zhou and J. J. Zhao, Physical properties and device applications of graphene oxide, *Front. Phys.*, 2020, **15**, 33301.

15 Y. Sun, S. Yang, G. Zhao, Q. Wang and X. Wang, Adsorption of Polycyclic Aromatic Hydrocarbons on Graphene Oxides and Reduced Graphene Oxides, *Chem. – Asian J.*, 2013, **8**, 2755.

16 T. Wen, X. Wu, X. Tan, X. Wang and A. Xu, One-Pot Synthesis of Water-Swellable Mg–Al Layered Double Hydroxides and Graphene Oxide Nanocomposites for Efficient Removal of As(V) from Aqueous Solutions, *ACS Appl. Mater. Interfaces*, 2013, **5**, 3304.

17 G. Duran-Jimenez, T. Monti, J. J. Titman, V. Hernandez-Montoya, S. W. Kingman and E. R. Binner, New insights into microwave pyrolysis of biomass: Preparation of carbon-based products from pecan nutshells and their application in wastewater treatment, *J. Anal. Appl. Pyrolysis*, 2017, **124**, 113.

18 V. Kirubakaran, V. Sivaramakrishnan, R. Nalini, T. Sekar, M. Premalatha and P. Subramanian, A review on gasification of biomass, *Renewable Sustainable Energy Rev.*, 2019, **13**, 179.

19 R. Pareja-Rodríguez, Y. Freile-Pelegrín, D. Robledo, M. Ruiz-Gómez, R. Martínez-Flores and G. Rodríguez-Gattorno, Self-generated active sites in graphene oxide-like materials by controlling the oxidative decomposition reactions of Sargassum, *J. Environ. Chem. Eng.*, 2021, **9**, 106551.

20 Q. Shi, G. E. Sterbinsky, V. Prigiobbe and X. Meng, Mechanistic Study of Lead Adsorption on Activated Carbon, *Langmuir*, 2018, **34**, 13565.

21 G. Kresse and J. Hafner, Ab initio molecular-dynamics simulation of the liquid-metal–amorphous-semiconductor transition in germanium, *Phys. Rev. B: Condens. Matter Mater. Phys.*, 1994, **49**, 14251.

22 G. Kresse and J. Furthmüller, Efficiency of ab-initio total energy calculations for metals and semiconductors using a plane-wave basis set, *Comput. Mater. Sci.*, 1996, **6**, 15.

23 G. Kresse and J. Furthmüller, Efficient iterative schemes for ab initio total-energy calculations using a plane-wave basis set, *Phys. Rev. B: Condens. Matter Mater. Phys.*, 1996, **54**, 11169.

24 P. E. Blochl, Projector augmented-wave method, *Phys. Rev. B: Condens. Matter Mater. Phys.*, 1994, **50**, 17953.

25 G. Kresse and D. Joubert, From ultrasoft pseudopotentials to the projector augmented-wave method, *Phys. Rev. B: Condens. Matter Mater. Phys.*, 1999, **59**, 1758.

26 J. P. Perdew, K. Burke and M. Ernzerhof, Generalized Gradient Approximation Made Simple, *Phys. Rev. Lett.*, 1996, **77**, 3865.

27 S. Grimme, J. Antony, S. Ehrlich and H. Krieg, A consistent and accurate ab initio parametrization of density functional dispersion correction (DFT-D) for the 94 elements H-Pu, *J. Chem. Phys.*, 2010, **132**, 154104.

28 H. Monkhorst and J. Pack, Special points for Brillouin-zone integrations, *Phys. Rev. B: Solid State*, 1976, **13**, 5188.

29 A. Otero-de-la-Roza, E. R. Johnson and V. Luaña, Critic2: A program for real-space analysis of quantum chemical

This journal is © The Royal Society of Chemistry 2024

Environ. Sci.: Nano, 2024, **11**, 4372–4380 | **4379**

interactions in solids, *Comput. Phys. Commun.*, 2014, **185**, 1007.

30 J. M. Galicia-Hernández, E. Chigo Anota, M. T. Romero de la Cruz, M. González Melchor and G. Hernández Cocoletzi, First principles studies of the graphene-phenol interactions, *J. Mol. Model.*, 2012, **18**, 3857.

31 J. I. Paez-Ornelas, H. N. Fernandez-Escamilla, H. A. Borbón-Nuñez, H. Tiznado, T. Noboru and J. Guerrero-Sánchez, A first-principles study of the atomic layer deposition of ZnO on carboxyl functionalized carbon nanotubes: the role of water molecules, *Phys. Chem. Chem. Phys.*, 2021, **23**, 3467.

32 G. X. Qian, R. M. Martin and D. J. Chadi, First-principles study of the atomic reconstructions and energies of Ga- and As-stabilized GaAs(100) surfaces, *Phys. Rev. B: Condens. Matter Mater. Phys.*, 1988, **38**, 7649.

33 J. Ruiz-González, G. H. Cocoletzi and L. Morales de la Garza, Modeling the Electronic structure and stability of three aluminum nitride phases, *Rev. Mex. Fis.*, 2021, **67**, 343.

34 S. J. Gutiérrez-Ojeda, R. Ponce-Pérez, J. Guerrero-Sánchez, R. García-Diaz, F. Sánchez-Ochoa, Ma. G. Moreno-Armenta and G. H. Cocoletzi, Modeling the half-metallicity of the CrN/GaN (111) heterostructure, *Appl. Surf. Sci.*, 2021, **566**, 150637.

35 O. Siidra, D. Nekrasova, W. Depmeier, N. Chukanov, A. Zaitsev and R. Turner, Hydro-cerussite-related minerals and materials: structural principles, chemical variations and infrared spectroscopy, *Acta Crystallogr., Sect. B: Struct. Sci., Cryst. Eng. Mater.*, 2018, **74**, 182.

36 E. R. Johnson, S. Keinan, P. Mori-Sánchez, J. Contreras-García, A. J. Cohen and W. Yang, Revealing Noncovalent Interactions, *J. Am. Chem. Soc.*, 2010, **132**, 6498.

37 J. Contreras-García, E. R. Johnson, S. Keinan, R. Chaudret, J. P. Piquemal, D. N. Beratan and W. Yang, NCIPLOT: A Program for Plotting Noncovalent Interaction Regions, *J. Chem. Theory Comput.*, 2011, **7**, 625.

38 Y. Wang, D. C. Alsmeyer and R. L. Mccreery, Raman Spectroscopy of Carbon Materials: Structural Basis of Observed Spectra, *Chem. Mater.*, 1990, **2**, 557.

39 L. Burgio, R. J. H. Clark and S. Firth, Raman spectroscopy as a means for the identification of plattnerite (PbO2), of lead pigments and of their degradation products, *Analyst*, 2001, **126**, 222.

40 W. Peng, H. Li, Y. Liu and S. Song, Comparison of Pb(II) adsorption onto graphene oxide prepared from natural graphites: Diagramming the Pb(II) adsorption sites, *Appl. Surf. Sci.*, 2016, **364**, 620.

41 E. Fiorito, G. E. Porcedda, L. Brundu, C. Passiu, D. Atzei, G. Ennas, B. Elsener, M. Fantauzzi and A. Rossi, Calcium carbonate as sorbent for lead removal from wastewaters, *Chemosphere*, 2022, **296**, 133897.

42 Z. Guo, J. Zhang, Y. Kang and H. Liu, Rapid and efficient removal of Pb(II) from aqueous solutions using biomass-derived activated carbon with humic acid in-situ modification, *Ecotoxicol. Environ. Saf.*, 2017, **145**, 442.

43 H. Wang, A. Zhou, F. Peng, H. Yu and J. Yang, Mechanism study on adsorption of acidified multiwalled carbon nanotubes to Pb(II), *J. Colloid Interface Sci.*, 2017, **316**, 277.

44 Z. Guo, P. Zhang, C. Xie, E. Voyiatzis, K. Faserl, A. J. Chetwynd, F. A. Monikh, G. Melagraki, Z. Zhang, W. J. G. M. Peijnenburg, A. Afantitis and C. Chen, Iseult Lynch, Defining the Surface Oxygen Threshold That Switches the Interaction Mode of Graphene Oxide with Bacteria, *ACS Nano*, 2023, **17**, 6350.

45 A. Alfarra, E. Frackowiak and F. Béguin, The HSAB concept as a means to interpret the adsorption of metal ions onto activated carbons, *Appl. Surf. Sci.*, 2004, **228**, 84.

4380 | *Environ. Sci.: Nano*, 2024, **11**, 4372–4380

This journal is © The Royal Society of Chemistry 2024